Flow past a slippery cylinder

Serge D'Alessio

Faculty of Mathematics,
University of Waterloo, Canada

EFMC12, September 9-13, 2018, Vienna, Austria

Introduction
- Problem description and background

Governing equations
- Conformal mapping
- Boundary conditions

Analytical solution procedure
- Rescaled equations
- Asymptotic expansion

Numerical solution procedure
- Fourier series decomposition

Results
- Circular cylinder
- Elliptic cylinder

Conclusions

The unsteady, laminar, two dimensional flow of a viscous incompressible fluid past a cylinder has been investigated analytically and numerically subject to impermeability and slip conditions for small to moderately large Reynolds numbers. Two geometries were considered: the circular cylinder and an inclined elliptic cylinder.

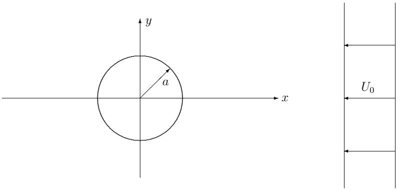

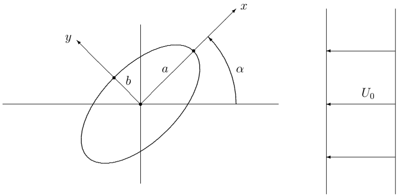

Some background information:

- There has been a lot work published for the no-slip case while very little for the slip case
- The no-slip condition is known to fail for: flows of rarified gases, flows within microfluidic / nanofluidic devices, and flows involving hydrophobic surfaces
- The widely used Beavers and Joseph [1967] semi-empirical slip condition was implemented in this study

In dimensionless form and in Cartesian coordinates the governing Navier-Stokes equations can be compactly formulated in terms of the stream function, ψ, and vorticity, ω:

$$\frac{\partial^2 \psi}{\partial x^2} + \frac{\partial^2 \psi}{\partial y^2} = \zeta$$

$$\frac{\partial \zeta}{\partial t} = \frac{\partial \psi}{\partial y}\frac{\partial \zeta}{\partial x} - \frac{\partial \psi}{\partial x}\frac{\partial \zeta}{\partial y} + \frac{2}{R}\left(\frac{\partial^2 \zeta}{\partial x^2} + \frac{\partial^2 \zeta}{\partial y^2}\right)$$

where R is the Reynolds number.

Introduce the conformal transformation $x + iy = H(\xi + i\theta)$ which transforms the infinite region exterior to the cylinder to the semi-infinite rectangular strip $\xi \geq 0$, $0 \leq \theta \leq 2\pi$. The governing equations become:

$$\frac{\partial^2 \psi}{\partial \xi^2} + \frac{\partial^2 \psi}{\partial \theta^2} = M^2 \zeta$$

$$M^2 \frac{\partial \zeta}{\partial t} = \frac{\partial \psi}{\partial \theta} \frac{\partial \zeta}{\partial \xi} - \frac{\partial \psi}{\partial \xi} \frac{\partial \zeta}{\partial \theta} + \frac{2}{R} \left(\frac{\partial^2 \zeta}{\partial \xi^2} + \frac{\partial^2 \zeta}{\partial \theta^2} \right)$$

For the circular cylinder:

$$H(\xi + i\theta) = \exp(\xi + i\theta) \ , \ M^2 = \exp(2\xi)$$

while for the elliptic cylinder:

$$H(\xi + i\theta) = \cosh[(\xi + \xi_0) + i\theta] \ , \ M^2 = \frac{1}{2}[\cosh[2(\xi + \xi_0)] - \cos(2\theta)$$

where $\tanh \xi_0 = r$ with r denoting the aspect ratio.

The conformal transformation for the elliptic cylinder is illustrated below:

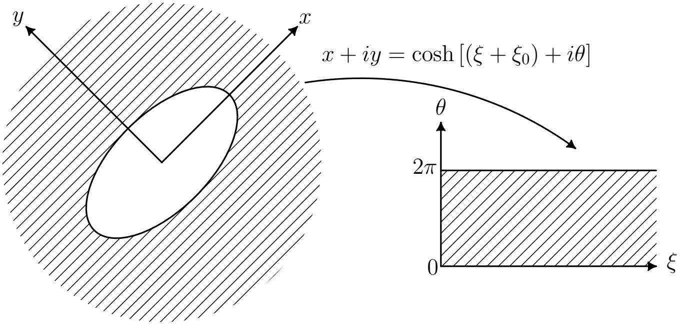

The velocity components (u, v) can be obtained using

$$u = -\frac{1}{M}\frac{\partial \psi}{\partial \theta} \; , \; v = \frac{1}{M}\frac{\partial \psi}{\partial \xi}$$

and the vorticity is related to these velocity components through

$$\zeta = \frac{1}{M^2}\left[\frac{\partial}{\partial \xi}(Mv) - \frac{\partial}{\partial \theta}(Mu)\right]$$

The surface boundary conditions include the impermeability and Navier-slip conditions given by

$$u = 0 \; , \; v = \beta \frac{\partial v}{\partial \xi} \text{ at } \xi = 0$$

where β denotes the slip length.

In terms of ψ and ζ these conditions become

$$\psi = 0 \ , \ \frac{\partial \psi}{\partial \xi} = \left(\frac{\beta M_0^4}{M_0^2 + \frac{\beta}{2} \sinh(2\xi_0)} \right) \zeta \text{ at } \xi = 0$$

In addition, we have the periodicity conditions

$$\psi(\xi, \theta, t) = \psi(\xi, \theta + 2\pi, t) \ , \ \zeta(\xi, \theta, t) = \zeta(\xi, \theta + 2\pi, t)$$

and the far-field conditions

$$\psi \to \mathrm{e}^{\xi} \sin\theta \text{ (circular cylinder)}$$

$$\psi \to \frac{1}{2} \mathrm{e}^{\xi + \xi_0} \sin(\theta + \alpha) \text{ (elliptic cylinder)}$$

$$\zeta \to 0 \text{ as } \xi \to \infty$$

To adequately resolve the impulsive start and early flow development we introduce the boundary-layer coordinate z and rescale the flow variables according to

$$\xi = \lambda z \ , \ \psi = \lambda \Psi \ , \ \zeta = \omega / \lambda \ \text{ where } \ \lambda = \sqrt{\frac{8t}{R}}$$

The governing equations transform to

$$\frac{\partial^2 \Psi}{\partial z^2} + \lambda^2 \frac{\partial^2 \Psi}{\partial \theta^2} = M^2 \omega$$

$$\frac{1}{M^2}\frac{\partial^2 \omega}{\partial z^2} + 2z\frac{\partial \omega}{\partial z} + 2\omega = 4t\frac{\partial \omega}{\partial t} - \frac{\lambda^2}{M^2}\frac{\partial^2 \omega}{\partial \theta^2} - \frac{4t}{M^2}\left(\frac{\partial \Psi}{\partial \theta}\frac{\partial \omega}{\partial z} - \frac{\partial \Psi}{\partial z}\frac{\partial \omega}{\partial \theta}\right)$$

Illustration of boundary-layer coordinates expanding with time: t_1 (left) and $t_2 > t_1$ (right).

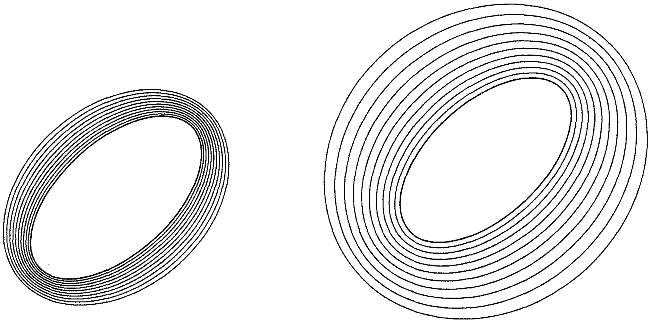

For small times and large Reynolds numbers both λ and t will be small. Based on this we can expand the flow variables in a double series in terms of λ and t. First we expand Ψ and ω in a series of the form

$$\Psi = \Psi_0 + \lambda\Psi_1 + \lambda^2\Psi_2 + \cdots$$

$$\omega = \omega_0 + \lambda\omega_1 + \lambda^2\omega_2 + \cdots$$

and then each $\Psi_n, \omega_n, n = 0, 1, 2, \cdots$, is further expanded in a series

$$\Psi_n(z, \theta, t) = \Psi_{n0}(z, \theta) + t\Psi_{n1}(z, \theta) + \cdots$$

$$\omega_n(z, \theta, t) = \omega_{n0}(z, \theta) + t\omega_{n1}(z, \theta) + \cdots$$

We note that when performing a double expansion the internal orders of magnitudes between the expansion parameters should be taken into account. Here, λ and t will be equal when $t = 8/R$, and thus, for a fixed value of R the procedure is expected to be valid for times that are of order $1/R$ provided that R is sufficiently large. The following leading-order non-zero terms in the expansions have been determined:

$$\Psi \sim \Psi_{00} + \lambda\, \Psi_{10}\ ,\ \omega \sim \lambda\, \omega_{10} + \lambda^2\, \omega_{20}$$

This approximate solution will be used to validate the numerical solution procedure.

The flow variables are expanded in a truncated Fourier series of the form:

$$\Psi(z,\theta,t)=\frac{F_0(z,t)}{2}+\sum_{n=1}^{N}[F_n(z,t)\cos(n\theta)+f_n(z,t)\sin(n\theta)]$$

$$\omega(z,\theta,t)=\frac{G_0(z,t)}{2}+\sum_{n=1}^{N}[G_n(z,t)\cos(n\theta)+g_n(z,t)\sin(n\theta)]$$

The resulting differential equations for the Fourier coefficients are then solved by finite differences subject to the boundary and far-field conditions. The computational parameters used were:

$$z_\infty=10\ ,\ N=25\ ,\Delta z=0.05\ ,\ \Delta t=0.01\ ,\ \varepsilon=10^{-6}$$

For the circular cylinder the flow is completely characterized by the Reynolds number, R, and the slip length, β. For the no-slip case ($\beta = 0$) comparisons in the drag coefficient, C_D, were made with documented results:

R	Reference	C_D
40	Present (unsteady, $t = 25$)	1.612
	Dennis & Chang [1970] (steady)	1.522
	Fornberg [1980] (steady)	1.498
	D'Alessio & Dennis [1994] (steady)	1.443
100	Present (unsteady, $t = 25$)	1.195
	Dennis & Chang [1970] (steady)	1.056
	Fornberg [1980] (steady)	1.058
	D'Alessio & Dennis [1994] (steady)	1.077

Comparison in surface vorticity distribution for $R = 1,000$ and $\beta = 0.5$.
Numerical - solid line
Analytical - dashed line

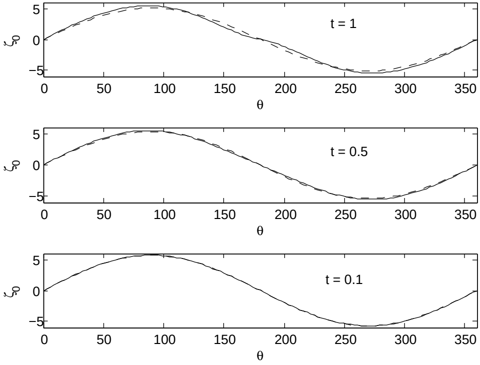

Streamline plots at $t = 15$ for $R = 500$ and $\beta = 0, 0.1, 0.5, 1$ from top to bottom, respectively.

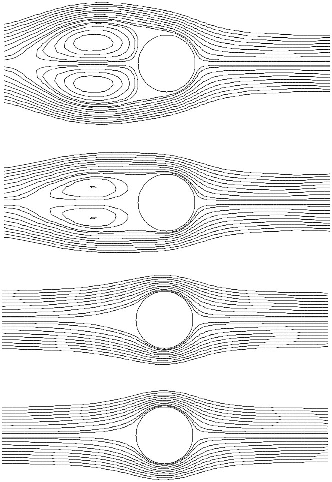

Time variation of C_D for $R = 500$ and $\beta = 0, 0.1, 0.5, 1.$

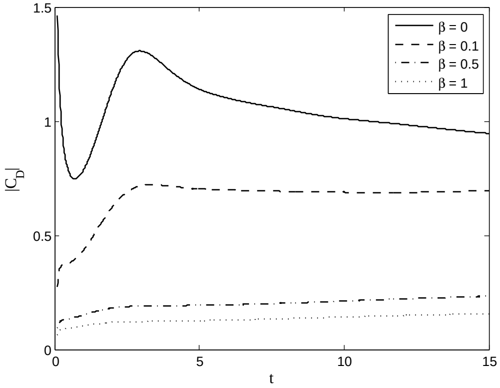

The distribution of the pressure coefficient, P^*, at $t = 15$ for $R = 500$ and $\beta = 0, 0.1, 0.5, 1$.

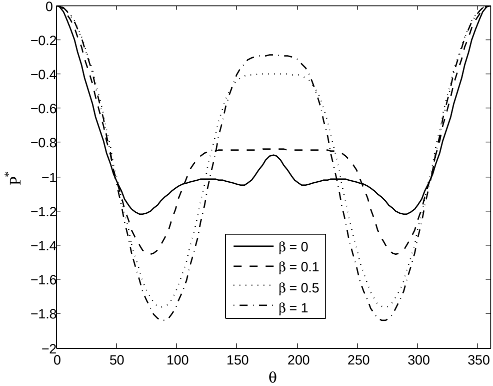

Streamline plots for $R = 1,000$ at $t = 1, 2, 5, 10$ from top to bottom, respectively, with $\beta = 0$ (left) and $\beta = 1$ (right).

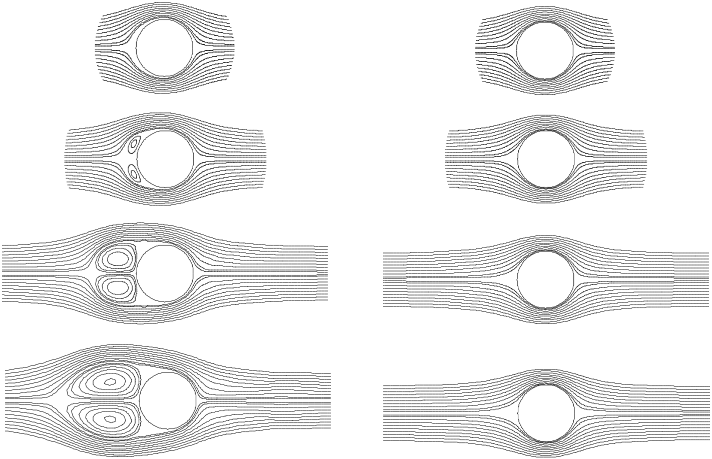

For the elliptic cylinder the flow is completely characterized by the Reynolds number, R, the slip length, β, the inclination, α, and the aspect ratio, r. For the no-slip case ($\beta = 0$) comparisons in the drag and lift coefficients (C_D, C_L) were made with documented results for $R = 20$ and $r = 0.2$:

	Dennis & Young [2003] (steady)		D'Alessio & Dennis [1994] (steady)		Present (unsteady, $t = 10$)	
α	C_D	C_L	C_D	C_L	C_D	C_L
20°	1.296	0.741	1.305	0.751	1.382	0.737
40°	1.602	0.947	1.620	0.949	1.786	0.985
60°	1.911	0.706	1.931	0.706	2.228	0.748

Comparison in $|C_D|$, C_L between present (solid line) and Staniforth [1972] (dashed line) no-slip results for the case $R = 6,250$, $r = 0.6$ and $\alpha = 15^\circ$.

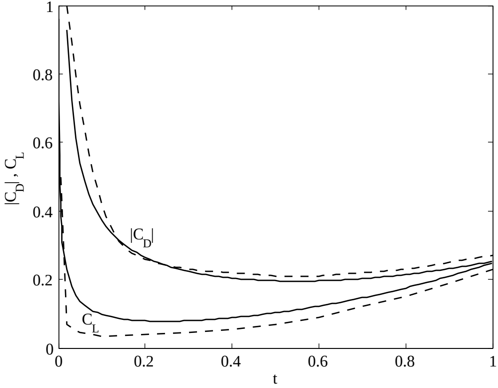

Comparison in surface vorticity distributions for the case $R = 1,000$, $\beta = 0.5$, $\alpha = 45^\circ$ and $r = 0.5$.
Numerical - solid line
Analytical - dashed line

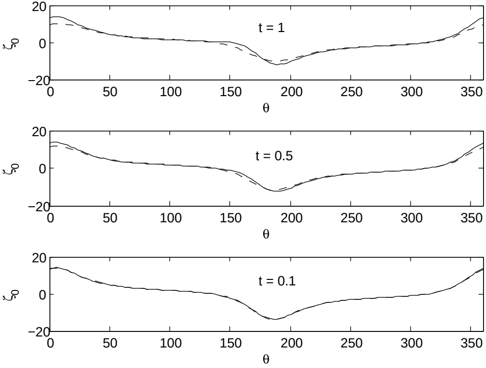

Streamline plots for $R = 500$, $r = 0.5$, $\alpha = 45^\circ$ and $\beta = 0$ at selected times $t = 0.65, 0.75, 1, 3, 5, 9, 10$ from top to bottom, respectively.

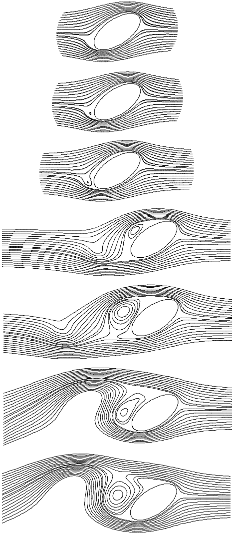

Time variation in $|C_D|$, C_L for the case $R = 500$, $r = 0.5$, $\alpha = 45^\circ$ and $\beta = 0$.

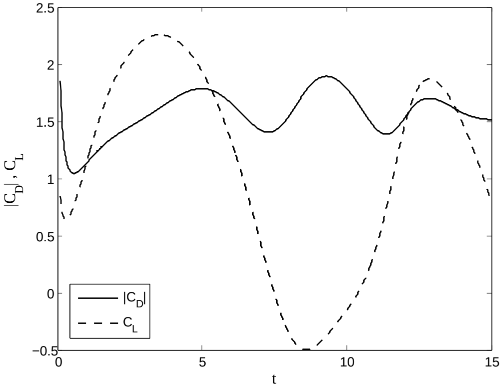

Time variation in $|C_D|$ for the cases $R = 500$, $r = 0.5$, $\alpha = 45^\circ$ and $\beta = 0, 0.25, 0.5$.

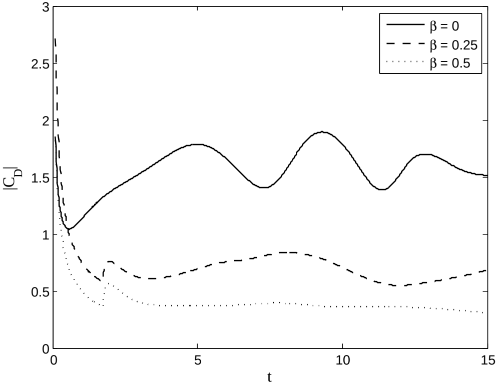

Time variation in C_L for the cases $R = 500$, $r = 0.5$, $\alpha = 45^\circ$ and $\beta = 0, 0.25, 0.5$.

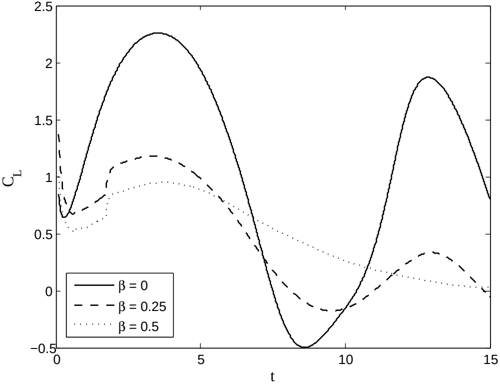

Streamline plots for $R = 500$, $r = 0.5$ and $\alpha = 45^\circ$ at $t = 3, 5, 7, 9, 10, 15$ from top to bottom, respectively, with $\beta = 0.25$ (left) and $\beta = 0.5$ (right).

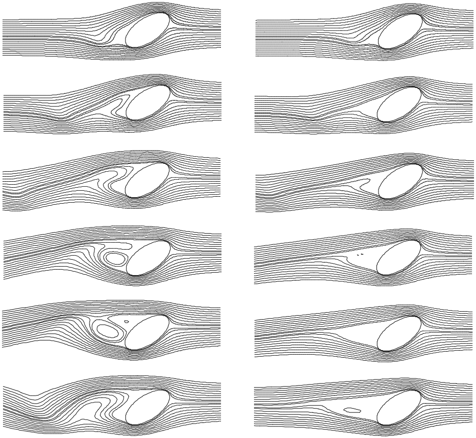

Surface vorticity distributions at $t = 15$ for $R = 500$, $r = 0.5$ and $\alpha = 45^\circ$ with $\beta = 0, 0.25, 0.5$.

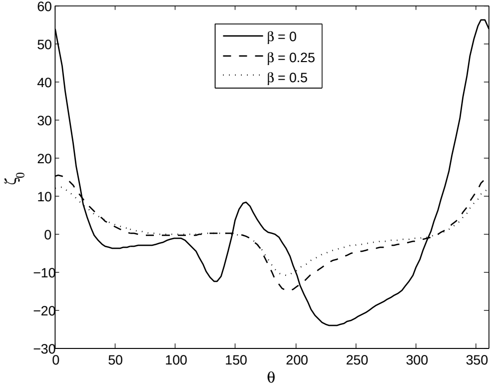

- Slip flow past a cylinder was investigated analytically and numerically
- Circular and elliptic cylinders were considered over a small to moderately large Reynolds number range
- Excellent agreement between the analytical and numerical solutions was found
- Good agreement with previous studies for the no-slip case was also found
- The slip condition was observed to suppress flow separation and vortex shedding
- The key finding is a reduction in drag when compared to the corresponding no-slip case
- For more details see the papers:
  Acta Mechanica, **229**, 3375 - 3392, 2018
  Acta Mechanica, **229**, 3415 - 3436, 2018